

# Data-Efficient Operator Learning via Unsupervised Pretraining and In-Context Learning

Wuyang Chen<sup>\*,1,2</sup>, Jialin Song<sup>\*,1,2</sup>, Pu Ren<sup>3</sup>, Shashank Subramanian<sup>3</sup>,  
Dmitriy Morozov<sup>3</sup>, Michael W. Mahoney<sup>1,2,3</sup>

<sup>1</sup> Department of Statistics, University of California, Berkeley

<sup>2</sup> International Computer Science Institute

<sup>3</sup> Lawrence Berkeley National Laboratory

## Abstract

Recent years have witnessed the promise of coupling machine learning methods and physical domain-specific insight for solving scientific problems based on partial differential equations (PDEs). However, being data-intensive, these methods still require a large amount of PDE data. This reintroduces the need for expensive numerical PDE solutions, partially undermining the original goal of avoiding these expensive simulations. In this work, seeking data efficiency, we design unsupervised pretraining and in-context learning methods for PDE operator learning. To reduce the need for training data with simulated solutions, we pretrain neural operators on unlabeled PDE data using reconstruction-based proxy tasks. To improve out-of-distribution performance, we further assist neural operators in flexibly leveraging in-context learning methods, without incurring extra training costs or designs. Extensive empirical evaluations on a diverse set of PDEs demonstrate that our method is highly data-efficient, more generalizable, and even outperforms conventional vision-pretrained models.

## 1 Introduction

Recent advancements in machine learning methodology have shown promise in solving partial differential equations (PDEs) [1–8]. A significant development in this area is the concept of operator learning for PDEs. This approach differs from traditional neural network methods, which are restricted to fixed-dimension input and output, since neural operators focus on learning mappings between function spaces [3–5]. As with other neural network methods, neural operators are recognized to be universal approximators for any continuous operator [3, 9], enabling them to approximate any physical operator, including solution operators for various parametric PDE families. A solution operator is defined as a function that maps physical inputs (e.g., initial conditions) to output solutions. Previous work has shown that in simple settings neural operators can effectively capture complex, multi-scale dynamic processes [4, 9–11].

However, neural operator methods tend to suffer from a problem common to other DNN methods, namely the **need for enormous quantities of data**. The relatively limited availability of data is a common problem in science and engineering. High-fidelity numerical simulations are computationally costly or even infeasible for many applications [12]. For example, an extreme-scale simulation of magnitude 7.0 earthquake at frequencies up to 10 Hz in the San Francisco requires 3600 Summit GPU nodes and 42.7 hour [13].

Motivated by these data-efficiency challenges, recent work in machine learning, in particular natural language processing (NLP) and computer vision (CV), has focused on two general strategies for reducing the cost of collecting or generating labeled data for training: unsupervised (self-supervised) pretraining<sup>1</sup>; and in-context (few-shot) learning.

---

\*Equal contribution.

<sup>1</sup>In this paper, we use the terms “unsupervised pretraining” and “self-supervised pretraining” interchangeably.

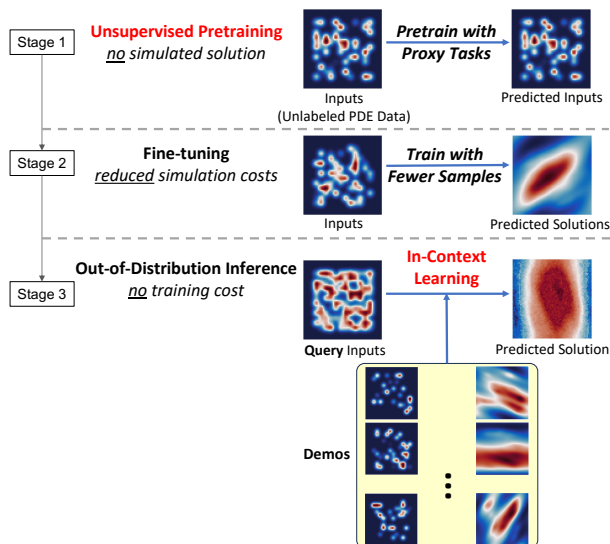


Figure 1: Overview of our framework for data-efficient neural operator learning (with our contributions highlighted in red). Stage 1: Unsupervised pretraining only on unlabeled PDE data. Stage 2: Fine-tuning with reduced simulation costs of PDE data. Stage 3: Test-time in-context learning to improve the neural operator’s out-of-distribution performance, without additional training costs.

**Unsupervised Pretraining.** Unsupervised pretraining is widely used in CV and NLP to “pretrain” models. Such pretrained models have been shown to be highly data-efficient in downstream fine-tuning [14], and they can even become few-shot learners without any downstream data [15]. In CV, people collect large amounts of natural images without any manual labels, and they then pretrain visual encoders with proxy tasks, such as Noise-Contrastive Estimation (NCE) [16], masked reconstruction [17], or rotation or jigsaw prediction [18, 19]. In NLP, people typically pretrain models via next-word prediction or masked tokens [15, 20]. However, unsupervised pretraining is still largely under-explored in Scientific Machine Learning (SciML). Therefore, our first question is:

*Q1: How can we design unsupervised pretraining for operator learning to reduce the data simulation costs?*

**In-Context Learning (ICL).** In-context learning (ICL) is a process by which a language model can make predictions on a test sample based on only a few demonstration examples provided in the input context [15, 21]. It is one of the most fascinating capabilities of large language models (LLMs), as this feature makes LLMs particularly versatile and adaptive to different downstream tasks—in particular for out-of-distribution (OOD) tasks, where only a limited number of downstream examples are needed, and without any fine-tuning cost. Recently, ICL has been introduced to operator learning. For example, during training, Yang et al. [22, 23] enable the model to leverage a few provided support examples (or “demonstrations”) via self-attention, thus facilitating ICL when making predictions on OOD samples. However, this particular implementation of ICL, which introduces extra training costs as well as an explicit number of few-shot examples, deviates from the successful ICL practice in NLP, where language models are trained with simple token-prediction tasks and can easily scale up to *any* number of few-shot examples during inference. Therefore, our second question is:

*Q2: How can we design a simple ICL for neural operators to achieve data-efficient OOD generalization?*

In this work, to achieve data efficiency in SciML, we propose unsupervised pretraining and ICL for neural operator learning. We overview our framework in Figure 1. To start, we propose two reconstruction-based proxy tasks. We demonstrate that with unsupervised pretraining, our neural operators not only improve counterparts trained with more simulated data, but also outperform off-the-shelf pretrained checkpoints from other popular domains (such as CV). Then, to further improve the data efficiency during OOD inference, we design a simple ICL strategy that is flexible and can scale up to any number of unseen supporting examples (“demos”). This approach also introduces zero overhead during training: one just keeps the standard training pipeline, and our ICL can be seamlessly plugged in (without further fine-tuning) for data-efficient OOD

inference. In more detail, we summarize our main contributions:

1. We introduce unsupervised pretraining for data-efficient neural operator learning. We show that unsupervised pretraining on unlabeled PDE data can achieve better performance than models trained with more simulated data and publicly-available checkpoints pretrained on other benchmarks (such as CV), demonstrating the importance of pretraining on PDE domain data.
2. We propose a flexible ICL approach that can improve the OOD generalization of neural operators, without introducing any extra costs during training.
3. We provide a detailed empirical evaluation on diverse PDE benchmarks, demonstrating that we can achieve significant savings in PDE simulations and improve the performance of neural operators in OOD contexts.

## 2 Related Works

### 2.1 Machine Learning for Scientific Modeling

There has been a long history of using machine learning-based methods to model (often nonlinear) physical scientific phenomena [24–27]. A representative line of work is so-called physics-informed neural networks (PINNs) [2, 28–31], which try to incorporate physics in neural networks by including the differential form of the PDE as an additional physics loss regularization term. However, this paradigm is confined to specific PDE scenarios (e.g., fixed PDE coefficients) instead of being more physics-agnostic. Moreover, recent work has highlighted fundamental issues with PINN-based methods [32, 33]. On the other hand, operator learning methods, including Fourier Neural Operators [3–5] and Deep Operator Network [6], have achieved progress in approximating the solution operators of PDEs. Although these data-driven approaches show promise in learning PDE solutions, they (like many neural network-based methods) rely on vast quantities of high-fidelity labeled data. For operator learning, such data are usually computationally expensive to simulate [2, 34, 35].

### 2.2 Unsupervised Pretraining and Foundation Models

Unsupervised (or self-supervised) pretraining is a key method in CV and NLP to achieve meaningful representations [14], data-efficient fine-tuning [36], and foundation models [37]. In CV, contrastive learning learns meaningful features by distinguishing between similar (positive) and different (negative) samples [14, 16, 38–40]. Masked Autoencoder (MAE) [17] uses a reconstructive approach where parts of the input are masked and the model learns to predict masked parts. In NLP, among the most prominent works are large language models (LLMs) such as GPT [15, 41, 42] and BERT [20], which leverage next token prediction for pretraining. The remarkable abilities [43] exhibited by foundation LLMs underscore the critical role of scale in achieving advanced capabilities that are not evident at smaller scales.

Similar directions also show progress in SciML. Brandstetter et al. [34] and Mialon et al. [44] propose to create augmented views in the solution space via Lie Symmetries. Most notably, Subramanian et al. [11] study the scaling behavior of supervised pretraining and OOD generalization, charting directions for foundational models for SciML. Lanusse et al. [45] targets learning astronomical foundation models with cross-modal contrastive learning. McCabe et al. [46] builds large task-agnostic models with a broad understanding of common physical behavior to serve as foundation models for SciML.<sup>2</sup>

### 2.3 In-Context Learning

In-context learning is a promising paradigm in deep learning that helps deep networks generalize to unseen domains with a few in-context examples. Early works in computer vision seek to learn feature-level correspondence between the target and a few “shots,” such that models can generalize to open-set unseen

---

<sup>2</sup>As with others efforts motivated by the goal of foundational models for SciML, the data and scaling used in this paper certainly lack sufficient diversity to categorize the resulting models as “foundational.” However, our work marks the first extensive implementation of successful multiple nonlinear physics pretraining for spatiotemporal systems.

objects [47, 48]. In NLP, people find large language models (LLMs) are naturally few-shot learners [15], and thus tuning or optimizing prompts becomes extremely important to improve the in-context learning performance of LLMs [49, 50]. More recently, within SciML, a different operator learning strategy, termed “in-context operator learning,” has been proposed [22, 23]. During both training and inference, the neural operator is asked to make predictions by explicitly leveraging so-called “demo” examples (pairs of physical parameters and simulated solutions). This approach provides a balance between model generalization and addressing data scarcity in the scenario of OOD testing.

### 3 Methods

In this section, we introduce our framework (outlined in Figure 1). We propose to first pretrain the model with unsupervised pretraining (Sec. 3.1), which will contribute to the data efficiency and reduced PDE simulation costs during standard training of neural operators. When we move to OOD scenarios during inference, we test our models with ICL (Sec. 3.2) to avoid further fine-tuning costs.

#### 3.1 Unsupervised Pretraining

The core idea in unsupervised (or self-supervised) pretraining is to train a neural network with properly designed proxy tasks. These proxy tasks are unsupervised, i.e., they do not require labeled data, but they are designed to be highly related to the supervised learning objectives of interest. While popular in CV and NLP, unsupervised pretraining on unlabeled data has never been explored in PDE operator learning in SciML, mainly due to two unresolved questions: 1) What kinds of unlabeled data can we use to train neural operators? 2) How can we design proxy tasks for PDE data? We address each of these questions in turn.

##### 3.1.1 Unlabeled Data

In SciML, neural operators are trained to map physical parameters and initial conditions to PDE solutions [4, 6]. Therefore, as a general approach to pretraining neural operators without labels (simulations), we will only use information in unlabeled PDE data.

**Unlabeled PDE Data.** Our unlabeled PDE data is a broader concept of related inputs in modeling PDE systems. Let us consider the second-order linear differential equation as a general example. It is formulated as

$$\sum_{i,j=1}^n a_{ij}(x)u_{x_i x_j} + \sum_{i=1}^n b_i(x)u_{x_i} + c(x)u = f(x),$$

where  $x \in \mathbb{R}^n$  represents physical space that varies in different systems ( $n = 3$  for 2D time-dependent PDEs); the coefficients (or physical parameters)  $a_{ij}, b_i, c$  are known from the physical process;  $u$  is the target solution; and  $f$  denotes an external forcing function [51]. We can consider two situations:

- Time-independent equations: following previous works [4, 11], our unlabeled PDE data include physical parameters ( $a_{ij}, b_i, c$ ), forcing functions ( $f$ ), and coordinates (grids of the discrete physical space).
- Time-dependent equations (e.g., forecasting problems [10, 46]): without simulating the temporal dynamics, our unlabeled PDE data include initial snapshot  $u_0(x)$ , which is sufficient for defining PDE systems.

There are two main reasons for pretraining only on unlabeled PDE data, as discussed below.

**Cheap Generation of Unlabeled PDE Data.** Only generating unlabeled PDE data and snapshots without temporal dynamics will be much cheaper than simulating solutions, making our unsupervised pretraining highly feasible in practice. This pretraining strategy will be very data-efficient and can avoid the high computational cost of simulating complex time-dependent equations for massive high-fidelity labeled solutions (Table 8).

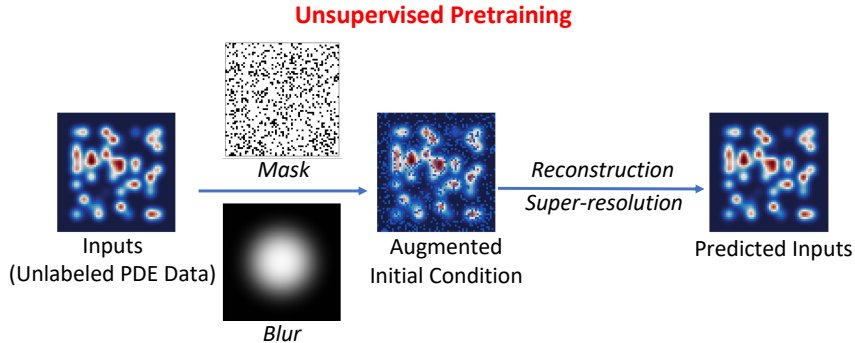


Figure 2: Overview of unsupervised pretraining via MAE and super-resolution. During pre-training, in the input unlabeled PDE data, a random subset of spatial locations of (e.g., 70%) is masked out, followed by a Gaussian blur. After the encoder and decoder, the full set of input is required to be reconstructed.

**Benefits of Pretraining on Unlabeled PDE Data.** Beyond the cheap generation, pretraining on unlabeled PDE data has the following benefits. First, *regularization against overfitting in the low-data regime*. When training on extremely low volumes of data, neural operators tend to overfit with poor generalization. Instead, unsupervised pretraining can strongly regularize the model towards better generalization, without the need for any early-stopping heuristics. Second, *more meaningful representations*. Pretraining on unlabeled PDE data can help models extract useful representations for subsequent operator learning. We defer our results and experimental details in Figure 4 in Sec. 4.1.

### 3.1.2 Proxy Tasks

To illustrate our general approach of constructing proxy tasks, we choose two variants of reconstruction as our core proxy tasks. In particular, we will input unlabeled PDE data to our neural operators, and after a decoder network we will force the output to be close to the input. We consider two perturbation variants (or augmented views).

**Masked Autoencoder.** Masked autoencoders (MAEs) have been shown to be scalable self-supervised learners [17]. The method is conceptually simple: remove a portion of the input data, and learn to predict the removed content. These methods enable training in NLP and CV of generalizable models containing over one hundred billion parameters [15, 20]. Here, we investigate the potential of MAE for scientific modeling.

The motivation for using MAEs is that PDE dynamics are invariant to sparse sensing of the full field scientific data [52, 52, 53]. We enforce our model to learn sensor invariance via random masking, and we extract the invariant features over distorted views of the same unlabeled PDE data. The invariance to sparse sensing of scientific data will facilitate the robustness of the representations from MAE.

Therefore, we consider MAE as a proxy task. Specifically, our MAE is a straightforward autoencoding approach that reconstructs the original signal, given its partial observation. Like all autoencoders, our approach has an encoder that maps the observed signal to a latent representation, and a decoder that reconstructs the original signal from the latent representation. We randomly sample masks according to a certain masking ratio (i.e., the ratio of removed areas), and the values of masked areas of unlabeled PDE data are set to zero. Our loss function computes the mean squared error (MSE) between the reconstructed and original input. We compute the loss only on masked areas; if no mask is applied (i.e., a vanilla autoencoder), the MSE loss will be applied to all spatial areas.

**Super-resolution.** Super-resolution (SR) techniques have emerged as powerful tools for enhancing data resolution, improving the overall quality and fidelity of data representation, and retrieving fine-scale structures.

SR is a task that involves recovering fine-scale data from corresponding coarse-grained data. It is also a popular task on PDE learning [54, 55].

The motivation for using SR is that numerical solutions of PDEs are expected to exhibit invariance to filtering blur or different resolutions of initial conditions [56, 57]. For instance, in turbulence simulations, the traditional numerical methods always fail to model the expected physical phenomenon with low-resolution meshes due to substantial numerical errors. SR has emerged as a powerful tool for subgrid modeling of PDE dynamics, especially helping to capture the critical patterns of turbulence [56, 58].

Therefore, we introduce SR as another proxy task. Specifically, we enforce the model to learn resolution-invariant features and to generate invariant features of the unlabeled PDE data which are immune to resolution and blur. To do so, we apply a Gaussian filter to blur the unlabeled PDE data, and the autoencoder will reconstruct the high-resolution unlabeled PDE data. Instead of applying a fixed blurring, we randomly sample the variance of the Gaussian filter from a certain range as augmentations.

### 3.1.3 PDEs

After pretraining on unlabeled PDE data, we fine-tune neural operators on simulated solutions of PDEs. We study two time-independent PDEs (Poisson, Helmholtz) and two time-dependent PDEs (Reaction-Diffusion, Navier-Stokes). We include details of these PDEs in Appendix A.

### 3.1.4 Model Architectures

We consider two popular architectures for fair comparisons with previous works. These are encoder-decoder architectures designed to reconstruct the original input given partial observations, where the encoder maps observed unlabeled PDE data to a latent space, and the decoder reconstructs the original conditions.

**Fourier Neural Operator.** Fourier Neural Operator (FNO) targets learning PDE data in the Fourier space. The original model backbone (encoder) employs Fourier transform and learns lower Fourier modes with linear transforms. The FNO backbone outputs features back to the spatial domain (i.e., the embeddings are on the pixel level). We refer readers to the original paper for details [4, 9].

- *Pretraining:* We build the decoder to be identical to the encoder (except for the input/output dimension). Unlabeled PDE data are randomly masked at the pixel level.
- *Fine-tuning:* After the pretraining, we discard the decoder, and we follow the original design to append two fully-connected layers (with ReLU activations) to predict final spatial-wise solutions.

**Transformer.** Transformers, which mainly employ self-attention and linear transform blocks, have shown promise in both NLP and CV [59, 60]. Different from FNO, which directly operates on grids, transformers tokenize and group grids into patches, i.e., each tokenized patch embeds a local neighborhood of subgrids. We follow the 3D transformer architecture of Video-MAE [46, 61]. Our encoder embeds patches by a linear projection with added positional embeddings (just as in a standard ViT), and it then processes the resulting set via a series of Transformer blocks. For the transformer, the unlabeled PDE data are randomly masked at the patch level.

- *Pretraining:* For the transformer encoder, we only apply it on the subset of tokens that are visible (i.e., unmasked patches), and masked patches are removed. This allows us to train encoders efficiently. The input to the MAE decoder is the full set of tokens consisting of (i) encoded visible patches, and (ii) the mask token. The mask token is a shared and learned vector that indicates the presence of a missing patch to be predicted. We add positional embeddings to all tokens in this full set. Without this, mask tokens would have no information about their location in the input. Following [17, 61], we adopt an asymmetric design where the decoder is more lightweight (shallower and narrower) than the encoder.
- *Fine-tuning:* After the pretraining, the decoder is preserved during fine-tuning, since we need to reconstruct the tokenized patches back to the input.

### 3.2 In-Context Learning

Out-of-distribution (OOD) generalization is a critical technical challenge, not only in SciML but also across multiple domains in AI for science [35]. To improve the OOD generalizability of neural operators and to reduce the extra effort of downstream fine-tuning, the following inference paradigm has been proposed: given a query input, the model is also provided with a few supporting examples (dubbed “demos”), together with their ground-truth solutions, to make the final prediction. This approach enables the “open-set” generalization of the model to make predictions on unseen samples.

Originally, in the literature on few-shot learning [48, 62–67], people developed delicate architectures to find a correspondence between the input and the supporting examples. The purpose of this extra architecture/training design is twofold: first, **find similarities** between the target input and supporting examples; and second, **aggregate labels** of supporting examples for the final predictions. Recent ICL works [22, 23] on learning PDE data also adopt this strategy, with transformers and cross-attention layers.

However, the ICL of LLMs enables a different strategy. The pretraining is still standard and simple (next/masked token prediction), without additional training costs. During inference, LLMs can autoregressively take any number of few-shot examples, finding similarities between tokens in few-shot examples and those in the target query (via self-attention), and then generate responses by aggregating embeddings of tokens in few-shot examples. This ICL strategy used in LLM is highly scalable and training-efficient.

Motivated by this, we propose our simple ICL for neural operators. We describe our method in Algorithm 1.

**Similarity by Prediction.** We find spatial-wise and temporal-wise similar demos by calculating their distance in the output space. That means, for two input locations over the spatial and temporal resolution, if we find their outputs of the trained neural operator similar, then we treat them as similar samples. We assume demos share the same distribution of physical parameters with the query.

**Aggregation.** For each spatial-temporal location of the query, after finding its similar samples in demos, we aggregate and average their solutions as the prediction.

---

**Algorithm 1:** Pseudocode of Test-time In-context Learning in a PyTorch-like style.

---

- 1 **Data resolution:** x-axis ( $W$ ), y-axis ( $H$ ), temporal steps ( $T$ ), channel dimensions for the input ( $C_{in}$ ) and solution ( $C_{out}$ ).
  - 2 **Input:** Query input ( $x \in \mathbb{R}^{H \times W \times C_{in}}$ ). Paired unlabeled PDE data ( $X \in \mathbb{R}^{J \times H \times W \times C_{in}}$ ) and solutions ( $Y \in \mathbb{R}^{J \times H \times W \times T \times C_{out}}$ ) as  $J$  demos. Trained Neural Operator Model  $\mathcal{M}$ . TopK ( $k$ ) demo solutions to aggregate.
  - 3  $\hat{y} = \mathcal{M}(x)$  ▷ Shape:  $H \times W \times T \times C_{out}$
  - 4  $\hat{Y} = \mathcal{M}(X)$  ▷ Shape:  $J \times H \times W \times T \times C_{out}$
  - 5  $\hat{\delta} = \hat{y}.\text{reshape}(-1, 1, C_{out}) - \hat{Y}.\text{reshape}(1, -1, C_{out})$  ▷ Shape:  $H \times W \times T \times (J \cdot H \cdot W \cdot T) \times C_{out}$
  - 6  $\hat{\delta} = \text{absolute}(\hat{\delta}).\text{sum}(-1)$
  - 7  $\text{index} = \text{argsort}(\hat{\delta}, -1)[:, :, :, : k]$  ▷ Spatial and temporal selection of demos similar to the query.
  - 8  $\hat{y}_{icl} = \text{take\_along\_dim}(\hat{Y}.\text{reshape}(-1, C_{out}), \text{index})$  ▷ Shape:  $H \times W \times T \times C_{out} \times k$ . Spatial and temporal aggregation of solutions from similar demos.
  - 9 **Return:**  $\hat{y}_{icl}.\text{mean}(-1)$
- 

## 4 Empirical Results

To illustrate the benefits of our approach, we perform empirical evaluations and address the following questions. *First*, does our unsupervised pretraining (on unlabeled PDE data, followed by fine-tuning) outperform neural operators trained from scratch, while requiring fewer PDE simulations (Sec. 4.1)? *Second*, does our in-context learning help the model generalize better to OOD cases (Sec. 4.2)?

In our experiments, we trained models three times with different random seeds and provided error bars. For more experimental details, please refer to Appendix B. We also include ablation studies about pretraining hyperparameters in Appendix C. For visualizations of our pretraining, please refer to Appendix D.

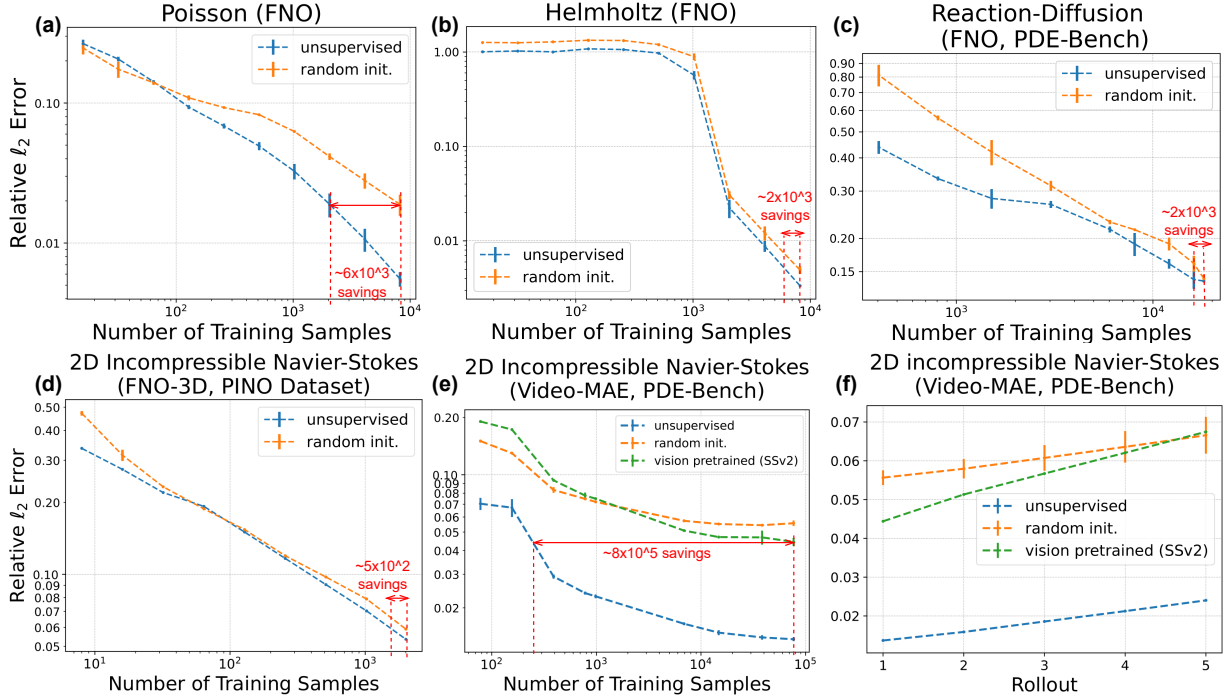


Figure 3: Pretraining neural operators on unlabeled PDE data improves its performance and data efficiency on Poisson (a), Helmholtz (b), Reaction-Diffusion (c), and Navier-Stokes (d and e, with relative errors at different unrolled steps shown on f). “random init.”: models are trained from scratch with random initialization. “vision pretrained (SSv2)”: fine-tuning from the publicly available checkpoint for Video-MAE (pretrained on computer vision dataset SSV2 [68] for video understanding). Savings of the number of simulated PDE data (when “random init.” achieves the best test error) are shown in red.

#### 4.1 Unsupervised Pretraining Enables Data-Efficient Operator Learning

**Data Efficiency.** We first demonstrate that, by leveraging unsupervised pretraining, neural operators can achieve improved relative errors with less simulated data. See Figure 3. We can see that, compared with directly training neural operators from scratch (“random init.”), pretraining on unlabeled PDE data can help neural operators achieve better performance, which can further help reduce the amount of simulated data. Specifically, in our experiments, when we target achieving the best test error of the baseline (“random init.”), our method can save  $5 \times 10^2 \sim 8 \times 10^5$  simulated solutions across diverse PDE systems.

Among all PDEs, we find that Helmholtz (Figure 3 (b)) is the most challenging. Two curves failed to improve the error until we increased the number of simulated data points to over 1024. Meanwhile, the generalization gaps remain high (Figure 4 (b)), indicating low training errors. We suspect that learning on the Helmholtz equation may be exhibiting the grokking issue [69, 70], where the network quickly memorizes the training data, but the improvement in generalizability is delayed.

**Unsupervised Pretraining Outperforms Off-the-Shelf Pretrained Checkpoints.** Pretraining on unlabeled PDE data is not the only way to save simulation costs. As pretraining is widely adopted in CV, pretrained checkpoints on vision data become publicly available. We choose to compare with Video-MAE [61] for state-of-the-art video understanding pretrained on CV dataset SSV2 [68]. As shown in Figure 3 (e), vision-pretrained Video-MAE can only outperform the random initialization with high volumes of simulated data, while its performance suffers when fine-tuned with limited simulations. In contrast, our unsupervised pretraining on unlabeled PDE data can save a significant amount of simulated data.

As errors during testing may quickly accumulate with further timestamps, we also report results with



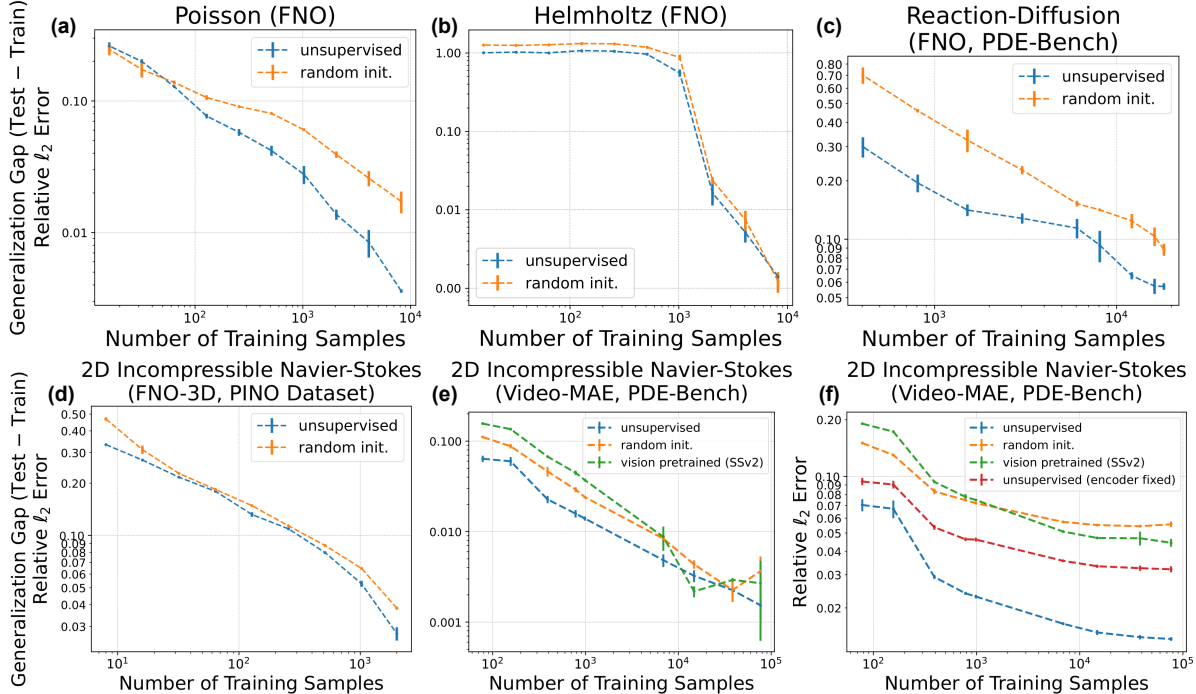


Figure 4: Benefits of unsupervised pretraining: 1) Universally reduced overfitting (i.e. smaller generalization gaps) on all PDEs (a to e); 2) Meaningful representations: pretraining Video-MAE with fixed encoder (red line) can extract meaningful features from unlabeled PDE data and outperform the baseline and the vision-pretrained model (f).

more unrolled steps. We use checkpoints trained with the largest amount of simulated data from above for this study. As shown in Figure 3 (f), at each rollout step, our unsupervised pretraining achieves much better performance. Similarly, vision-pretrained Video-MAE is eventually outperformed by the random initialization at the long rollout step.

**Benefits of Pretraining on Unlabeled PDE Data.** Pretraining on unlabeled PDE data is beneficial beyond achieving better performance with less simulated PDE data. *First*, we find that pretraining on unlabeled PDE data can strongly regularize the model against overfitting, without the need for any early-stopping heuristics (our smaller generalization gaps in Figure 4 (a-e)). *Second*, unsupervised pretraining can also help models extract useful representations for subsequent operator learning. For example, in Figure 4 (f), we find that with even pre-extracted features (i.e., model’s encoder is fixed during fine-tuning), our neural operators can still outperform baselines (trained from scratch).

## 4.2 ICL Enables Data-Efficient OOD Generalization

We now move to OOD settings, where models will be tested on PDE data simulated with physical parameters unseen during fine-tuning/training. Neural operators suffer from poor OOD generalization [11, 22]. Traditionally, improvements heavily depend on further fine-tuning on simulated data, which requires extra simulation and training costs. We study the benefits of our test-time in-context learning. As shown in Figure 5, when we flexibly scale up the number of demos, we can keep improving FNO’s OOD generalization on diverse PDEs. Notably, we introduce zero training overhead: we keep the standard training pipeline, and our ICL can be seamlessly plugged in during OOD inference.

We show visualizations of in-context learning in Figure 5. In this visualization, we find that the range of numerical solutions (e.g., values in colorbars) predicted by in-context learning become closer to the target. Please refer to Appendix F for further discussions about the benefits of ICL.

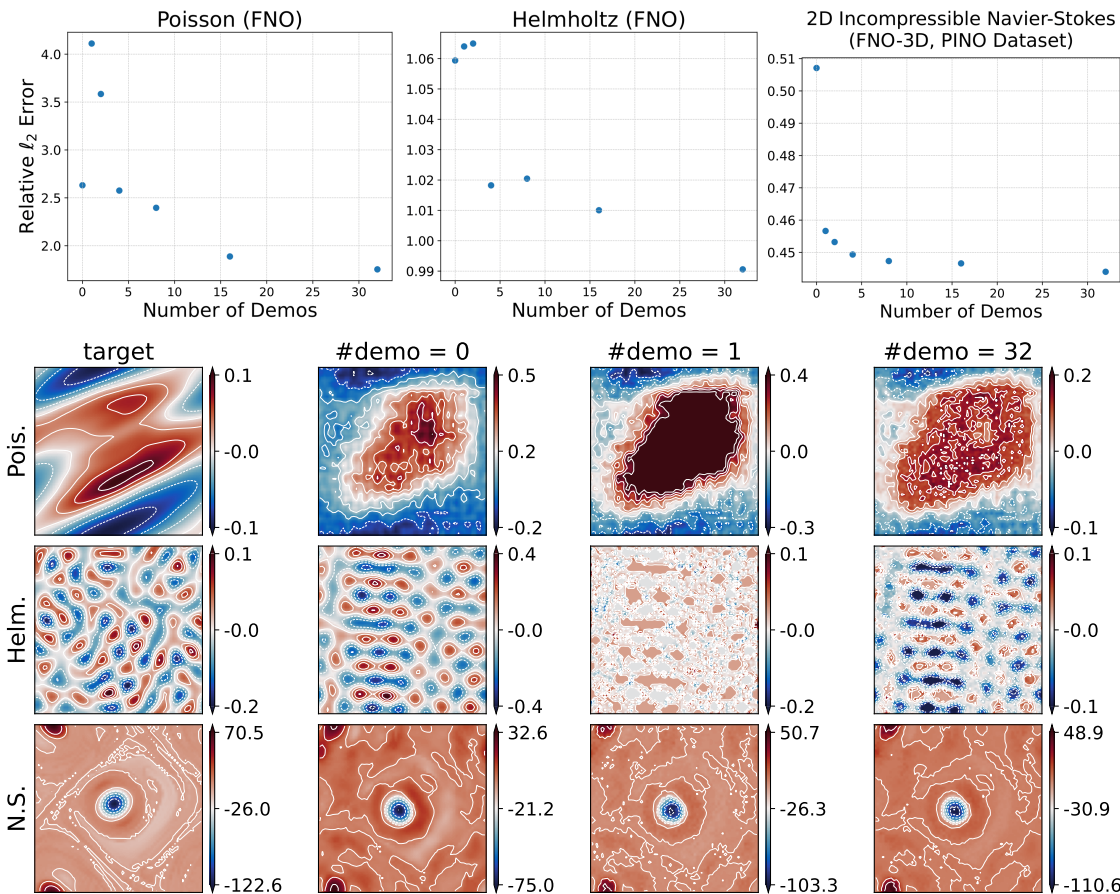


Figure 5: In-context learning for FNO in OOD testing. Top panel: relative  $\ell_2$  errors decrease as we increase the number of in-context demos. Bottom panel: visualizations, where ranges of solutions predicted by in-context learning (min/max of each snapshot, reflected in colorbars) become closer to the target.

## 5 Conclusion

In this work, we focus on enhancing the data efficiency of solving PDEs using deep neural networks, particularly through unsupervised pretraining and ICL methods. Current machine learning methods for PDEs are data-intensive, which can be expensive to obtain. Our key contributions include the introduction of unsupervised pretraining for neural operator learning and a flexible ICL approach that enhances OOD generalization without incurring extra training costs. Through extensive empirical evaluations, we demonstrate that our method is not only data-efficient but also more generalizable compared to existing approaches. We anticipate that our work would inspire the SciML community to explore more on solving the heavy simulation costs and unsatisfactory OOD generalization of neural operators.

## Acknowledgements

This work was supported by the U.S. Department of Energy, Office of Science, Office of Advanced Scientific Computing Research, Scientific Discovery through Advanced Computing (SciDAC) program, under Contract Number DE-AC02-05CH11231 at Lawrence Berkeley National Laboratory. This research used resources of the National Energy Research Scientific Computing Center (NERSC), a U.S. Department of Energy Office of Science User Facility located at Lawrence Berkeley National Laboratory, operated under Contract Number DE-AC02-05CH11231 using NERSC award ASCR-ERCAP0023337.

## References

- [1] Jiequn Han, Arnulf Jentzen, and Weinan E. Solving high-dimensional partial differential equations using deep learning. *Proceedings of the National Academy of Sciences*, 115(34):8505–8510, 2018.
- [2] Maziar Raissi, Paris Perdikaris, and George E Karniadakis. Physics-informed neural networks: A deep learning framework for solving forward and inverse problems involving nonlinear partial differential equations. *Journal of Computational Physics*, 378:686–707, 2019.
- [3] Nikola Kovachki, Zongyi Li, Burigede Liu, Kamyar Azizzadenesheli, Kaushik Bhattacharya, Andrew Stuart, and Anima Anandkumar. Neural operator: Learning maps between function spaces with applications to PDEs. *Journal of Machine Learning Research*, 24(89):1–97, 2023.
- [4] Zongyi Li, Nikola Borislavov Kovachki, Kamyar Azizzadenesheli, Burigede liu, Kaushik Bhattacharya, Andrew Stuart, and Anima Anandkumar. Fourier neural operator for parametric partial differential equations. In *International Conference on Learning Representations*, 2021.
- [5] Zongyi Li, Nikola Kovachki, Kamyar Azizzadenesheli, Burigede Liu, Andrew Stuart, Kaushik Bhattacharya, and Anima Anandkumar. Multipole graph neural operator for parametric partial differential equations. *Advances in Neural Information Processing Systems*, 33:6755–6766, 2020.
- [6] Lu Lu, Pengzhan Jin, and George Em Karniadakis. Deeponet: Learning nonlinear operators for identifying differential equations based on the universal approximation theorem of operators. *arXiv preprint arXiv:1910.03193*, 2019.
- [7] A. S. Krishnapriyan, A. F. Queiruga, N. B. Erichson, and M. W. Mahoney. Learning continuous models for continuous physics. *Communications Physics*, 6:319, 2023.
- [8] D. Hansen, D. C. Maddix, S. Alizadeh, G. Gupta, and M. W. Mahoney. Learning physical models that can respect conservation laws. *Physica D: Nonlinear Phenomena*, 457:133952, 2024.
- [9] Zongyi Li, Hongkai Zheng, Nikola Kovachki, David Jin, Haoxuan Chen, Burigede Liu, Kamyar Azizzadenesheli, and Anima Anandkumar. Physics-informed neural operator for learning partial differential equations. *arXiv preprint arXiv:2111.03794*, 2021.
- [10] Makoto Takamoto, Timothy Praditia, Raphael Leiteritz, Daniel MacKinlay, Francesco Alesiani, Dirk Pflüger, and Mathias Niepert. Pdebench: An extensive benchmark for scientific machine learning. *Advances in Neural Information Processing Systems*, 35:1596–1611, 2022.
- [11] Shashank Subramanian, Peter Harrington, Kurt Keutzer, Wahid Bhimji, Dmitriy Morozov, Michael W Mahoney, and Amir Gholami. Towards foundation models for scientific machine learning: Characterizing scaling and transfer behavior. *arXiv preprint arXiv:2306.00258*, 2023.
- [12] Justin Sirignano, Jonathan F MacArt, and Jonathan B Freund. Dpm: A deep learning pde augmentation method with application to large-eddy simulation. *Journal of Computational Physics*, 423:109811, 2020.
- [13] David McCallen, Anders Petersson, Arthur Rodgers, Arben Pitarka, Mamun Miah, Floriana Petrone, Bjorn Sjogreen, Norman Abrahamson, and Houjun Tang. Eqsim—a multidisciplinary framework for fault-to-structure earthquake simulations on exascale computers part i: Computational models and workflow. *Earthquake Spectra*, 37(2):707–735, 2021.
- [14] Ting Chen, Simon Kornblith, Mohammad Norouzi, and Geoffrey Hinton. A simple framework for contrastive learning of visual representations. In *International conference on machine learning*, pages 1597–1607. PMLR, 2020.

- [15] Tom Brown, Benjamin Mann, Nick Ryder, Melanie Subbiah, Jared D Kaplan, Prafulla Dhariwal, Arvind Neelakantan, Pranav Shyam, Girish Sastry, Amanda Askell, et al. Language models are few-shot learners. *Advances in neural information processing systems*, 33:1877–1901, 2020.
- [16] Aaron van den Oord, Yazhe Li, and Oriol Vinyals. Representation learning with contrastive predictive coding. *arXiv preprint arXiv:1807.03748*, 2018.
- [17] Kaiming He, Xinlei Chen, Saining Xie, Yanghao Li, Piotr Dollár, and Ross Girshick. Masked autoencoders are scalable vision learners. In *Proceedings of the IEEE/CVF conference on computer vision and pattern recognition*, pages 16000–16009, 2022.
- [18] Mehdi Noroozi and Paolo Favaro. Unsupervised learning of visual representations by solving jigsaw puzzles. In *European conference on computer vision*, pages 69–84. Springer, 2016.
- [19] Spyros Gidaris, Praveer Singh, and Nikos Komodakis. Unsupervised representation learning by predicting image rotations. *arXiv preprint arXiv:1803.07728*, 2018.
- [20] Jacob Devlin, Ming-Wei Chang, Kenton Lee, and Kristina Toutanova. Bert: Pre-training of deep bidirectional transformers for language understanding. *arXiv preprint arXiv:1810.04805*, 2018.
- [21] Robert L Logan IV, Ivana Balažević, Eric Wallace, Fabio Petroni, Sameer Singh, and Sebastian Riedel. Cutting down on prompts and parameters: Simple few-shot learning with language models. *arXiv preprint arXiv:2106.13353*, 2021.
- [22] Liu Yang, Siting Liu, Tingwei Meng, and Stanley J Osher. In-context operator learning with data prompts for differential equation problems. *Proceedings of the National Academy of Sciences*, 120(39): e2310142120, 2023.
- [23] Liu Yang, Tingwei Meng, Siting Liu, and Stanley J Osher. Prompting in-context operator learning with sensor data, equations, and natural language. *arXiv preprint arXiv:2308.05061*, 2023.
- [24] Isaac E Lagaris, Aristidis Likas, and Dimitrios I Fotiadis. Artificial neural networks for solving ordinary and partial differential equations. *IEEE transactions on neural networks*, 9(5):987–1000, 1998.
- [25] Isaac E Lagaris, Aristidis C Likas, and Dimitris G Papageorgiou. Neural-network methods for boundary value problems with irregular boundaries. *IEEE Transactions on Neural Networks*, 11(5):1041–1049, 2000.
- [26] Tianping Chen and Hong Chen. Universal approximation to nonlinear operators by neural networks with arbitrary activation functions and its application to dynamical systems. *IEEE transactions on neural networks*, 6(4):911–917, 1995.
- [27] Tianping Chen and Hong Chen. Approximation capability to functions of several variables, nonlinear functionals, and operators by radial basis function neural networks. *IEEE Transactions on Neural Networks*, 6(4):904–910, 1995.
- [28] Yin hao Zhu, Nicholas Zabaras, Phaedon-Stelios Koutsourelakis, and Paris Perdikaris. Physics-constrained deep learning for high-dimensional surrogate modeling and uncertainty quantification without labeled data. *Journal of Computational Physics*, 394:56–81, 2019.
- [29] Nicholas Geneva and Nicholas Zabaras. Modeling the dynamics of pde systems with physics-constrained deep auto-regressive networks. *Journal of Computational Physics*, 403:109056, 2020.
- [30] Han Gao, Luning Sun, and Jian-Xun Wang. Phygeonet: Physics-informed geometry-adaptive convolutional neural networks for solving parameterized steady-state pdes on irregular domain. *Journal of Computational Physics*, 428:110079, 2021.

- [31] Pu Ren, Chengping Rao, Yang Liu, Jian-Xun Wang, and Hao Sun. Phycrnet: Physics-informed convolutional-recurrent network for solving spatiotemporal pdes. *Computer Methods in Applied Mechanics and Engineering*, 389:114399, 2022.
- [32] Aditi Krishnapriyan, Amir Gholami, Shandian Zhe, Robert Kirby, and Michael W Mahoney. Characterizing possible failure modes in physics-informed neural networks. *Advances in Neural Information Processing Systems*, 34:26548–26560, 2021.
- [33] C. Edwards. Neural networks learn to speed up simulations. *Communications of the ACM*, 65(5):27–29, 2022.
- [34] Johannes Brandstetter, Max Welling, and Daniel E Worrall. Lie point symmetry data augmentation for neural pde solvers. In *International Conference on Machine Learning*, pages 2241–2256. PMLR, 2022.
- [35] Xuan Zhang, Limei Wang, Jacob Helwig, Youzhi Luo, Cong Fu, Yaochen Xie, Meng Liu, Yuchao Lin, Zhao Xu, Keqiang Yan, et al. Artificial intelligence for science in quantum, atomistic, and continuum systems. *arXiv preprint arXiv:2307.08423*, 2023.
- [36] Neil Houlsby, Andrei Giurgiu, Stanislaw Jastrzebski, Bruna Morrone, Quentin De Laroussilhe, Andrea Gesmundo, Mona Attariyan, and Sylvain Gelly. Parameter-efficient transfer learning for nlp. In *International Conference on Machine Learning*, pages 2790–2799. PMLR, 2019.
- [37] Rishi Bommasani, Drew A Hudson, Ehsan Adeli, Russ Altman, Simran Arora, Sydney von Arx, Michael S Bernstein, Jeannette Bohg, Antoine Bosselut, Emma Brunskill, et al. On the opportunities and risks of foundation models. *arXiv preprint arXiv:2108.07258*, 2021.
- [38] Yonglong Tian, Dilip Krishnan, and Phillip Isola. Contrastive multiview coding. In *Computer Vision—ECCV 2020: 16th European Conference, Glasgow, UK, August 23–28, 2020, Proceedings, Part XI 16*, pages 776–794. Springer, 2020.
- [39] Ishan Misra and Laurens van der Maaten. Self-supervised learning of pretext-invariant representations. In *Proceedings of the IEEE/CVF conference on computer vision and pattern recognition*, pages 6707–6717, 2020.
- [40] Kaiming He, Haoqi Fan, Yuxin Wu, Saining Xie, and Ross Girshick. Momentum contrast for unsupervised visual representation learning. In *Proceedings of the IEEE/CVF conference on computer vision and pattern recognition*, pages 9729–9738, 2020.
- [41] Alec Radford, Karthik Narasimhan, Tim Salimans, Ilya Sutskever, et al. Improving language understanding by generative pre-training. *OpenAI*, 2018.
- [42] Alec Radford, Jeffrey Wu, Rewon Child, David Luan, Dario Amodei, Ilya Sutskever, et al. Language models are unsupervised multitask learners. *OpenAI blog*, 1(8):9, 2019.
- [43] Jason Wei, Yi Tay, Rishi Bommasani, Colin Raffel, Barret Zoph, Sebastian Borgeaud, Dani Yogatama, Maarten Bosma, Denny Zhou, Donald Metzler, et al. Emergent abilities of large language models. *arXiv preprint arXiv:2206.07682*, 2022.
- [44] Grégoire Mialon, Quentin Garrido, Hannah Lawrence, Danyal Rehman, Yann LeCun, and Bobak T Kiani. Self-supervised learning with lie symmetries for partial differential equations. *arXiv preprint arXiv:2307.05432*, 2023.
- [45] Francois Lanusse, Liam Parker, Siavash Golkar, Miles Cranmer, Alberto Bietti, Michael Eickenberg, Geraud Krawezik, Michael McCabe, Ruben Ohana, Mariel Pettee, et al. Astroclip: Cross-modal pre-training for astronomical foundation models. *arXiv preprint arXiv:2310.03024*, 2023.

- [46] Michael McCabe, Bruno Régaldo-Saint Blancard, Liam Holden Parker, Ruben Ohana, Miles Cranmer, Alberto Bietti, Michael Eickenberg, Siavash Golkar, Geraud Krawezik, Francois Lanusse, et al. Multiple physics pretraining for physical surrogate models. *arXiv preprint arXiv:2310.02994*, 2023.
- [47] Li Fei-Fei, Robert Fergus, and Pietro Perona. One-shot learning of object categories. *IEEE transactions on pattern analysis and machine intelligence*, 28(4):594–611, 2006.
- [48] Xiaolin Zhang, Yunchao Wei, Yi Yang, and Thomas S Huang. Sg-one: Similarity guidance network for one-shot semantic segmentation. *IEEE transactions on cybernetics*, 50(9):3855–3865, 2020.
- [49] Yongchao Zhou, Andrei Ioan Muresanu, Ziwen Han, Keiran Paster, Silviu Pitis, Harris Chan, and Jimmy Ba. Large language models are human-level prompt engineers. *arXiv preprint arXiv:2211.01910*, 2022.
- [50] Alessandro Sordani, Xingdi Yuan, Marc-Alexandre Côté, Matheus Pereira, Adam Trischler, Ziang Xiao, Arian Hosseini, Friederike Niedtner, and Nicolas Le Roux. Deep language networks: Joint prompt training of stacked llms using variational inference. *arXiv preprint arXiv:2306.12509*, 2023.
- [51] AK Nandakumaran and PS Datti. *Partial differential equations: classical theory with a modern touch*. Cambridge University Press, 2020.
- [52] Steven L Brunton, Bernd R Noack, and Petros Koumoutsakos. Machine learning for fluid mechanics. *Annual Review of Fluid Mechanics*, 52:477–508, 2020.
- [53] N Benjamin Erichson, Lionel Mathelin, Zhewei Yao, Steven L Brunton, Michael W Mahoney, and J Nathan Kutz. Shallow neural networks for fluid flow reconstruction with limited sensors. *Proceedings of the Royal Society A*, 476(2238):20200097, 2020.
- [54] Wai Tong Chung, Bassem Akoush, Pushan Sharma, Alex Tamkin, Ki Sung Jung, Jacqueline Chen, Jack Guo, Davy Brouzet, Mohsen Talei, Bruno Savard, et al. Turbulence in focus: Benchmarking scaling behavior of 3d volumetric super-resolution with blastnet 2.0 data. In *Thirty-seventh Conference on Neural Information Processing Systems Datasets and Benchmarks Track*, 2023.
- [55] Pu Ren, N Benjamin Erichson, Shashank Subramanian, Omer San, Zarija Lukic, and Michael W Mahoney. Superbench: A super-resolution benchmark dataset for scientific machine learning. *arXiv preprint arXiv:2306.14070*, 2023.
- [56] Dmitrii Kochkov, Jamie A Smith, Ayya Alieva, Qing Wang, Michael P Brenner, and Stephan Hoyer. Machine learning–accelerated computational fluid dynamics. *Proceedings of the National Academy of Sciences*, 118(21):e2101784118, 2021.
- [57] Ricardo Vinuesa and Steven L Brunton. Enhancing computational fluid dynamics with machine learning. *Nature Computational Science*, 2(6):358–366, 2022.
- [58] Romit Maulik, Omer San, Adil Rasheed, and Prakash Vedula. Subgrid modelling for two-dimensional turbulence using neural networks. *Journal of Fluid Mechanics*, 858:122–144, 2019.
- [59] Ashish Vaswani, Noam Shazeer, Niki Parmar, Jakob Uszkoreit, Llion Jones, Aidan N Gomez, Lukasz Kaiser, and Illia Polosukhin. Attention is all you need. *Advances in neural information processing systems*, 30, 2017.
- [60] Alexey Dosovitskiy, Lucas Beyer, Alexander Kolesnikov, Dirk Weissenborn, Xiaohua Zhai, Thomas Unterthiner, Mostafa Dehghani, Matthias Minderer, Georg Heigold, Sylvain Gelly, et al. An image is worth 16x16 words: Transformers for image recognition at scale. *arXiv preprint arXiv:2010.11929*, 2020.
- [61] Zhan Tong, Yibing Song, Jue Wang, and Limin Wang. Videomae: Masked autoencoders are data-efficient learners for self-supervised video pre-training. *Advances in neural information processing systems*, 35: 10078–10093, 2022.

- [62] Xiaolin Zhang, Yunchao Wei, Guoliang Kang, Yi Yang, and Thomas Huang. Self-produced guidance for weakly-supervised object localization. In *Proceedings of the European conference on computer vision (ECCV)*, pages 597–613, 2018.
- [63] Juhong Min, Dahyun Kang, and Minsu Cho. Hypercorrelation squeeze for few-shot segmentation. In *Proceedings of the IEEE/CVF international conference on computer vision*, pages 6941–6952, 2021.
- [64] Xinyu Shi, Dong Wei, Yu Zhang, Donghuan Lu, Munan Ning, Jiashun Chen, Kai Ma, and Yefeng Zheng. Dense cross-query-and-support attention weighted mask aggregation for few-shot segmentation. In *European Conference on Computer Vision*, pages 151–168. Springer, 2022.
- [65] Dahyun Kang and Minsu Cho. Integrative few-shot learning for classification and segmentation. In *Proceedings of the IEEE/CVF Conference on Computer Vision and Pattern Recognition*, pages 9979–9990, 2022.
- [66] Jie Liu, Yanqi Bao, Guo-Sen Xie, Huan Xiong, Jan-Jakob Sonke, and Efstratios Gavves. Dynamic prototype convolution network for few-shot semantic segmentation. In *Proceedings of the IEEE/CVF Conference on Computer Vision and Pattern Recognition*, pages 11553–11562, 2022.
- [67] Bohao Peng, Zhuotao Tian, Xiaoyang Wu, Chengyao Wang, Shu Liu, Jingyong Su, and Jiaya Jia. Hierarchical dense correlation distillation for few-shot segmentation. In *Proceedings of the IEEE/CVF Conference on Computer Vision and Pattern Recognition*, pages 23641–23651, 2023.
- [68] Raghav Goyal, Samira Ebrahimi Kahou, Vincent Michalski, Joanna Materzynska, Susanne Westphal, Heuna Kim, Valentin Haenel, Ingo Fruend, Peter Yianilos, Moritz Mueller-Freitag, et al. The” something something” video database for learning and evaluating visual common sense. In *Proceedings of the IEEE international conference on computer vision*, pages 5842–5850, 2017.
- [69] Alethea Power, Yuri Burda, Harri Edwards, Igor Babuschkin, and Vedant Misra. Grokking: Generalization beyond overfitting on small algorithmic datasets. *arXiv preprint arXiv:2201.02177*, 2022.
- [70] Xuekai Zhu, Yao Fu, Bowen Zhou, and Zhouhan Lin. Critical data size of language models from a grokking perspective. *arXiv preprint arXiv:2401.10463*, 2024.
- [71] Gene A Klaasen and William C Troy. Stationary wave solutions of a system of reaction-diffusion equations derived from the fitzhugh–nagumo equations. *SIAM Journal on Applied Mathematics*, 44(1):96–110, 1984.
- [72] Aaron Defazio and Konstantin Mishchenko. Learning-rate-free learning by d-adaptation. *arXiv preprint arXiv:2301.07733*, 2023.

## A PDEs

We consider two time-independent PDEs (Poisson, Helmholtz) and two time-dependent PDEs (Reaction-Diffusion, Navier-Stokes), as described below.

1. *Poisson*: We consider a two-dimensional (2D) elliptic PDE that arises in various physical situations, with periodic boundary conditions within a spatial domain  $\Omega = [0, 1]^2$ :

$$-\operatorname{div} \mathbf{K} \nabla u = f \quad , \quad (1)$$

where  $u(x)$  represents the solution,  $f(x)$  acts as the source (e.g., forcing) function, and  $x$  denotes spatial coordinate. The diffusion coefficient tensor, denoted by  $\mathbf{K}$ , is employed to measure the physical properties of this system.

2. *Helmholtz*: We consider the 2D inhomogeneous Helmholtz equation, which is a time-independent form of the wave equation, with periodic boundary conditions and a spatial domain  $\Omega = [0, 1]^2$ . The governing equation is given by

$$-\Delta u + \omega u = f \quad \text{in } \Omega, \quad (2)$$

where  $u(x)$  denotes the solution,  $f(x)$  represents the source function, and  $\omega > 0$  is the wavenumber (that defines the dynamic properties of the Helmholtz equation). This system produces high-frequency large wavenumber oscillatory patterns, which poses challenges in terms of generalization.

3. *Reaction-Diffusion*: The 2D Reaction-Diffusion (RD) equation involves the interaction between two nonlinear coupled variables, i.e., the activator  $u(t, x, y)$  and the inhibitor  $v(t, x, y)$ . The RD equation is given by

$$\begin{aligned} \partial_t u &= D_u(\partial_{xx}u + \partial_{yy}u) + R_u, \\ \partial_t v &= D_v(\partial_{xx}v + \partial_{yy}v) + R_v, \end{aligned} \quad (3)$$

where  $\{D_u, D_v\}$  are diffusion coefficients for  $u$  and  $v$ , respectively, and where  $R_u$  and  $R_v$  are reaction functions, which are defined as the Fitzhugh-Nagumo equation [71]:

$$\begin{aligned} R_u &= u - u^3 - k - v, \\ R_v &= u - v. \end{aligned} \quad (4)$$

The spatial domain considered for the 2D RD equation is  $\Omega = [-1, 1]^2$ , and the time duration is  $t \in (0, 5]$ .

4. *Navier-Stokes Equation*: Lastly, we consider the 2D incompressible Navier-Stokes equation in vorticity form on the unit torus, which is formulated as

$$\begin{aligned} \partial_t w(x, t) + u(x, t) \cdot \nabla w(x, t) &= \nu \Delta w(x, t) + f(x), \\ \nabla \cdot u(x, t) &= 0, \\ w(x, 0) &= w_0(x). \end{aligned} \quad (5)$$

Here, the velocity  $u$  and the vorticity  $w$  are defined within the time duration  $[0, T]$  and the spatial domain  $[0, 1]^2$  (the vorticity can also be formulated as  $w = \nabla \times u$ ), and  $w_0$  is the initial vorticity. Moreover, the coefficient  $\nu$  signifies the viscosity of a fluid, and  $f(x)$  is the external forcing function. Periodic boundary conditions are employed in this system.

## B Detailed Experiment Settings

### B.1 Unlabeled PDE Data.

1. For Poisson and Helmholtz [4, 11], we consider coefficients, sourcing functions, and coordinates as unlabeled PDE data. These data are controlled by the physical parameters of PDE systems (diffusion coefficients, wavenumber).



- For the Diffusion-Reaction and Navier Stokes problems, we follow PINO [9] and PDEBench [10] to use snapshots without temporal dynamics as the unlabeled PDE data, controlled by diffusion coefficients and Reynolds number, respectively.

## B.2 Distributions of Unlabeled PDE Data.

In Table 1, we summarize the distribution of our unlabeled PDE data during pretraining, fine-tuning, and OOD inference with ICL. Ranges of these physical parameters are inspired by Subramanian et al. [11]. During pretraining, we consider a wide distribution of unlabeled PDE data. When training (fine-tuning) our model, we consider in-distribution unlabeled PDE data. Finally, we test our ICL method with OOD settings.<sup>3</sup> For Helmholtz OOD, we choose a narrow range of coefficients ([15, 20]) mainly because its solution is very sensitive to the wavenumber, and FNO’s performance significantly drops when we move to more extreme OOD settings.

Table 1: Ranges of physical parameters (integers) for unsupervised pretraining, training (fine-tuning), and out-of-distribution (OOD, for ICL).

Physics Parameters	Poisson (diffusion)	Helmholtz (wave number)	Naiver Stokes (Reynolds number)
Pretraining	[1, 20]	[1, 20]	{100, 300, 500, 800, 1000}
Training (or Fine-tuning)	[5, 15]	[5, 15]	300
Out-of-Distribution Testing	[15, 50]	[15, 20]	10000

## B.3 Hyperparameters

We summarize our hyperparameters used during pretraining and fine-tuning/training in Table 2. These hyperparameters strictly follow previous works [4, 9–11, 46].

Table 2: Hyperparameters for pretraining and training/fine-tuning. “N.S.”: 2D Incompressible Navier-Stokes. “DAdapt”: adaptive learning rate by D-adaptation [72]. “ns”: total number of simulated training samples.

Stage ↓	PDEs →	Poisson	Helmholtz	Reaction-Diffusion	N.S. (PINO)	N.S. (PDEBench)
Pretraining	Number of Samples	46,080	46,080	76,760	57,545	713,286
	Learning Rate	$1 \times 10^{-3}$	$1 \times 10^{-3}$	$1 \times 10^{-3}$	$1 \times 10^{-3}$	DAdapt
	Batch Size	32	32	5	2	8
	Resolution ( $H \times W$ )	64×64	64×64	128×128	128×128	512×512
	Epochs/Iterations	500 epochs	500 epochs	500 epochs	100,000 iters	500 epochs
Training/Fine-tuning	Learning Rate	$1 \times 10^{-3}$	$1 \times 10^{-3}$	$1 \times 10^{-3}$	$1 \times 10^{-3}$	DAdapt
	Batch Size	min(32, ns)	min(32, ns)	5	2	8
	Resolution ( $H \times W$ or $H \times W \times T$ )	64×64	64×64	128×128×10	64×64×1	512×512×15
	Epochs/Iterations	500 epochs	500 epochs	500 epochs	50,000 iters	500 epochs
	Rollouts	N/A	N/A	91	N/A	1

## C Ablation Studies

### C.1 Magnitude of Perturbations during Pretraining.

We study the optimal magnitude of perturbations during pretraining: “Mask Ratio” (1 indicates no visible grids, and 0 means no masks); and “Blur Sigma” for the variance of Gaussian kernel for blur (larger the more degradation). We show our results in Table 3, 4, 5, 6. For example, on 2D incompressible Navier-Stokes with FNO, as shown in Table 6, we can find that when training with a low volume of data, we should use much stronger perturbations (high masking ratios and strong blur), whereas a high volume of data only requires mild perturbations.

<sup>3</sup>For Navier Stokes from PDEBench, we use the original data. We could not generate our own pretraining/finetuning data with different ranges of physics parameters, due to a possible mismatch of the provided configuration files and the version of Phiflow used in PDEBench (see GitHub issue at <https://github.com/pdebench/PDEBench/issues/36>).

Table 3: Best choice of mask ratio and blur sigma for pretraining on Poisson equation.

#Samples	Mask Ratio	Blur Sigma
16	0	0
32	0	0~1
64	0	0~1
128	0	0~1
256	0	0~1
512	0	0~1
1024	0	0~1
2048	0	0~1
4096	0	0~1
8192	0	0~1

Table 4: Best choice of mask ratio and blur sigma for pretraining on Helmholtz equation.

#Samples	Mask Ratio	Blur Sigma
16	0.2	0~1
32	0.2	0~1
64	0.2	0~1
128	0.2	0~1
256	0.6	0~0
512	0.6	0~0
1024	0.6	0~0
2048	0	0~1
4096	0	0~1
8192	0	0~0.5

Table 5: Best choice of mask ratio and blur sigma for pretraining on 2D Diffusion-Reaction equation.

#Samples	Mask Ratio	Blur Sigma
404	0	0~1
808	0	0~1
1515	0	0~1
3030	7	0~2
6060	9	0~1
8080	3	0~1
12120	0	0~1
16160	0	0~1
18180	0	0~1

Table 6: Best choice of mask ratio and blur sigma for pretraining on 2D incompressible Navier-Stokes.

#Samples	Mask Ratio	Blur Sigma
8	0.7	0~4
16	0.7	0~4
32	0.7	0~4
64	0	0~1
128	0	0~1
256	0.05	0
512	0.05	0
1024	0.05	0
2000	0.05	0

## C.2 Ablation of the Number of Pretraining Samples.

As shown in Table 7, the more unlabeled PDE data we use for pretraining, the better quality the pretrained model will be.

Table 7: More unlabeled PDE data improve the quality of pretraining. FNO on 2D incompressible Navier-Stokes, pretrained with mask ratio as 0.7.

#Pretraining Samples	2000	57545
Relative $\ell_2$ Error	0.3594	0.3246

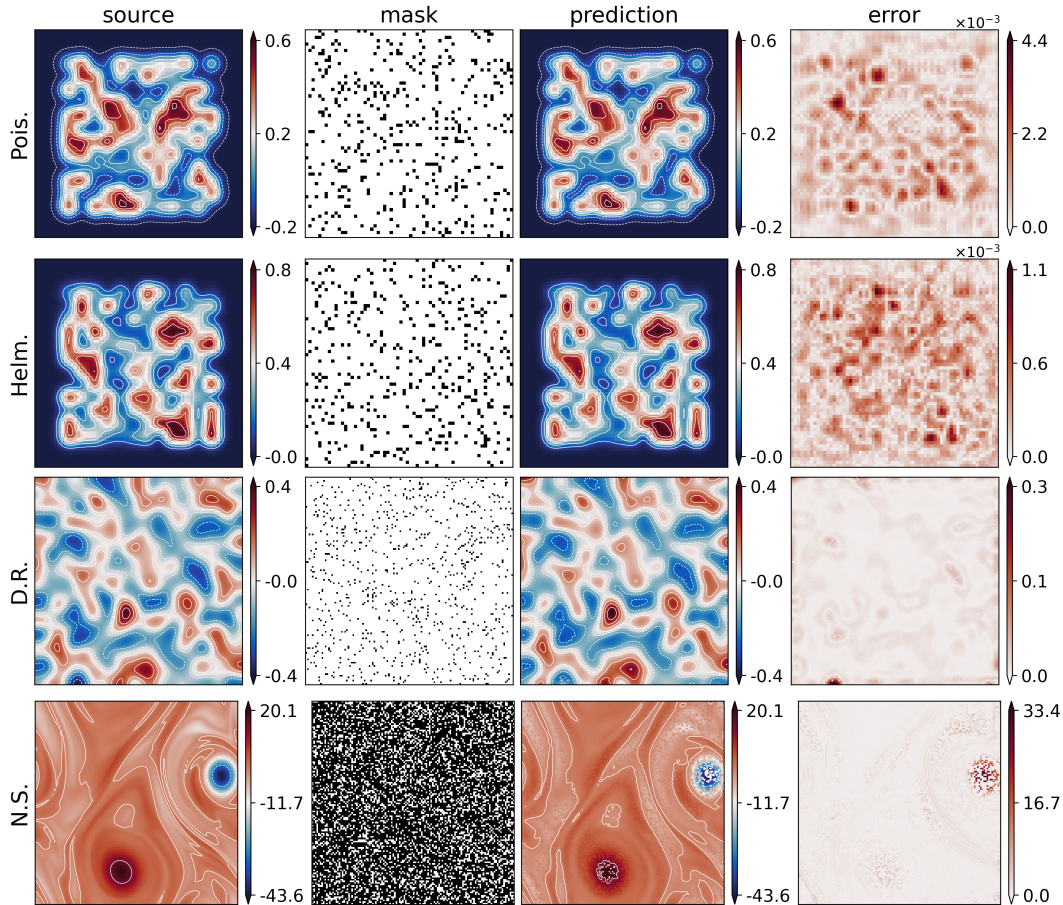


Figure 6: Visualization of reconstructions of unlabeled PDE data on the Poisson (“Pois.”), Helmholtz (“Helm.”), 2D Diffusion-Reaction (“D.R.”), and 2D incompressible Navier-Stokes (“N.S.”) equations during MAE pretraining. (Mask ratio: 0.1 for Poisson, Helmholtz, and 2D Diffusion-Reaction equations; 0.7 for incompressible Navier-Stokes.) In masks, only white areas are visible to the model during pretraining.

## D Visualization of MAE Pretraining

**MAE Pretraining on Different PDEs.** To demonstrate the efficacy of our MAE-based pretraining, we show the unlabeled PDE data and its reconstructed version in Figure 6 (MAE pretraining on different PDEs) and Figure 7 (MAE pretraining on 2D incompressible Navier-Stokes with varying mask ratios). We can see that all inputs are accurately reconstructed with low errors and similar patterns.

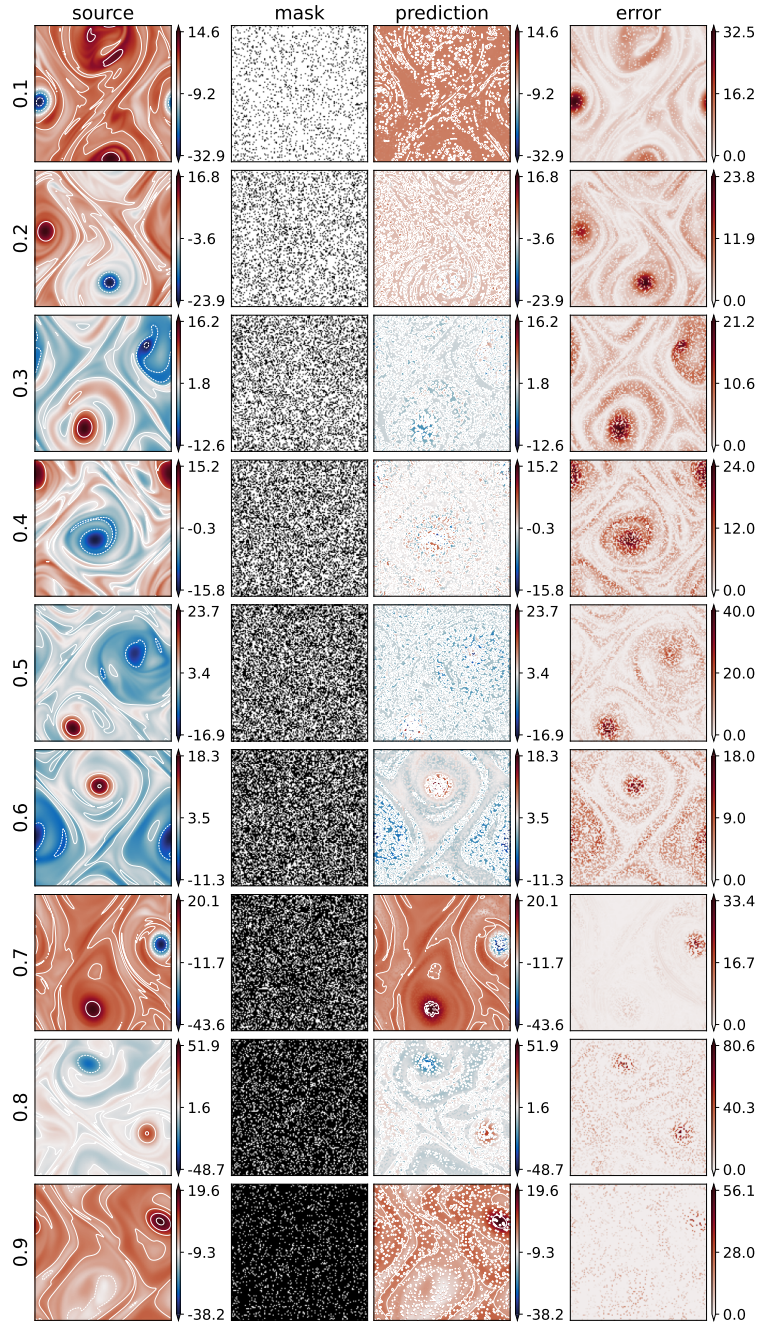


Figure 7: Visualization of reconstructions of unlabeled PDE data on the 2D incompressible Navier-Stokes equations during MAE pertaining with mask ratio from 0.1 to 0.9.

## E Example of Simulation Costs

In Table 8, we demonstrate the cheap simulation of only unlabeled PDE data, versus simulating both unlabeled PDE data and solutions, on 2D incompressible Navier-Stoke on PINO Dataset [9] and Reaction-Diffusion on PDE-Bench [10]. We can see that unlabeled PDE data are extremely cheap to simulate. Therefore, our

pretraining method can boost the performance and meanwhile save the heavy cost of data simulations.

Table 8: Simulation time costs on 2D Incompressible Navier-Stokes (“N.S.”) on PINO Dataset and Reaction-Diffusion (“R.D.”) on PDE-Bench. “ $Re$ ”: Reynolds number. “ $D_u, D_v$ ”: diffusion coefficients.

Data	Physical Parameters	Unlabeled PDE Data (s)	Data+Solutions (s)	Data Size	CPU	GPU
N.S.	$Re = 100$	5499.32	11013.90	$20 \times 100 \times 21 \times 512 \times 512$	1 AMD EPYC 7763	1 NVIDIA A100 (40GB)
	$Re = 300$	3683.02	7625.82			
	$Re = 500$	4059.71	8963.39			
	$Re = 800$	4829.3	10811.15			
	$Re = 1000$	4957.24	10788.69			
R.D.	$D_u = 1 \times 10^{-3}, D_v = 5 \times 10^{-3}$	29.65	6657.34	$1000 \times 101 \times 128 \times 128 \times 2$	1 AMD EPYC 7763	N/A

## F Benefits of In-context Learning (ICL)

We try to understand the benefit of ICL by decomposing the relative MSE error into “scale” and “shape.” “Scale” is the slope of a linear regression between targets and predictions (closer to 1 the better), indicating the alignment of the range of model outputs with targets. “Shape” is the normalized relative MSE (i.e., model outputs or targets are normalized by their own largest magnitude before MSE), indicating the alignment of scale-invariant spatial/temporal structures. We show results in Figure 8. We find that the benefit of ICL lies in that the scale of the model’s output keeps being better calibrated (“scale” being closer to 1) when adding more demos.

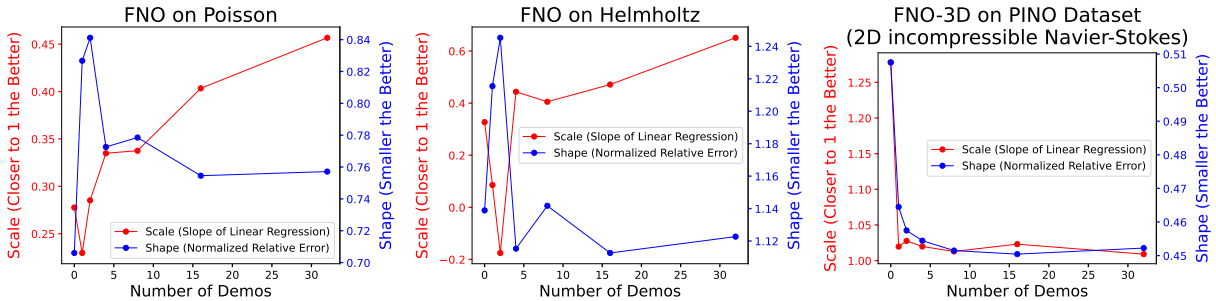


Figure 8: Benefits of ICL. To analyze the benefit of ICL in complicated PDE systems, we decompose the relative MSE error into “Scale” and “Shape”. “Scale” indicates the alignment of the range of model outputs with targets (closer to 1 the better), via the slope of a linear regression. “Shape” indicates the alignment of scale-invariant spatial/temporal structures via normalized relative MSE (i.e. model outputs or targets are normalized by their own largest magnitude before MSE). We find that the benefit of ICL lies in that the scale of the model’s output keeps being calibrated (red line being closer to 1) when adding more demos.